PARKINSON'S DISEASE

Pharmacological Rescue of Mitochondrial Deficits in iPSC-Derived Neural Cells from Patients with Familial Parkinson's Disease

Oliver Cooper,[1*†] Hyemyung Seo,[1*†‡] Shaida Andrabi,[2†] Cristina Guardia-Laguarta,[3†] John Graziotto,[4†] Maria Sundberg,[1†] Jesse R. McLean,[1†] Luis Carrillo-Reid,[5†] Zhong Xie,[5†] Teresia Osborn,[1†] Gunnar Hargus,[1†] Michela Deleidi,[1†] Tristan Lawson,[1†] Helle Bogetofte,[1†] Eduardo Perez-Torres,[1†] Lorraine Clark,[3†] Carol Moskowitz,[3†] Joseph Mazzulli,[4†] Li Chen,[2†] Laura Volpicelli-Daley,[6†] Norma Romero,[3†] Houbo Jiang,[7†] Ryan J. Uitti,[8†] Zhigao Huang,[9] Grzegorz Opala,[10] Leslie A. Scarffe,[2†] Valina L. Dawson,[2†] Christine Klein,[11] Jian Feng,[7†] Owen A. Ross,[8†] John Q. Trojanowski,[6†] Virginia M.-Y. Lee,[6†] Karen Marder,[3†] D. James Surmeier,[5†] Zbigniew K. Wszolek,[8†] Serge Przedborski,[3†] Dimitri Krainc,[4†] Ted M. Dawson,[2†] Ole Isacson[1†§]

Parkinson's disease (PD) is a common neurodegenerative disorder caused by genetic and environmental factors that results in degeneration of the nigrostriatal dopaminergic pathway in the brain. We analyzed neural cells generated from induced pluripotent stem cells (iPSCs) derived from PD patients and presymptomatic individuals carrying mutations in the *PINK1* (*PTEN-induced putative kinase 1*) and *LRRK2* (*leucine-rich repeat kinase 2*) genes, and compared them to those of healthy control subjects. We measured several aspects of mitochondrial responses in the iPSC-derived neural cells including production of reactive oxygen species, mitochondrial respiration, proton leakage, and intraneuronal movement of mitochondria. Cellular vulnerability associated with mitochondrial dysfunction in iPSC-derived neural cells from familial PD patients and at-risk individuals could be rescued with coenzyme Q_{10}, rapamycin, or the LRRK2 kinase inhibitor GW5074. Analysis of mitochondrial responses in iPSC-derived neural cells from PD patients carrying different mutations provides insight into convergence of cellular disease mechanisms between different familial forms of PD and highlights the importance of oxidative stress and mitochondrial dysfunction in this neurodegenerative disease.

INTRODUCTION

The progressive motor symptoms in Parkinson's disease (PD) involve the loss of particularly vulnerable dopaminergic (DA) synapses and neurons in the nigrostriatal pathway of the brain. There is also damage to other neurons in the central and peripheral nervous systems in PD. The reasons for loss of function and degeneration remain unclear, although the normal physiology of DA neurons (*1*, *2*) may be altered by hereditary genetic risk factors. Both genetic and environmental factors contribute to an individual's risk of developing PD (*3*–*6*). Over the past decade, mutations in several genes have been shown to confer a significant risk of developing PD (*7*, *8*). From studies of the rare inherited (familial) form of PD, mutations have been identified in the genes *leucine-rich repeat kinase 2* and *PTEN-induced putative kinase 1* encoding the LRRK2 and PINK1 kinases, respectively (*7*). Dominantly inherited mutations in *LRRK2* are associated with familial PD (*9*, *10*) that is clinically and pathologically similar, but not identical, to the more common late-onset idiopathic form of the disease (*11*–*14*). *LRRK2* pathogenic mutations occur in the catalytic domains of this kinase—the G2019S mutation in the kinase domain and the R1441C/G/H mutation in the guanosine triphosphatase domain—implicating altered LRRK2 kinase activity in PD pathogenesis (*15*, *16*). Mutations in *PINK1*, which encodes a mitochondria-targeted kinase, cause recessively inherited early-onset parkinsonism (*17*–*20*) that not only clinically resembles the common late-onset form of PD but also presents with additional psychiatric symptoms. It is not clear whether *PINK1* mutations cause the characteristic Lewy body inclusions that are found in most other forms of PD (*21*, *22*).

Patients with the common sporadic form of PD may have genetic variations that influence their risk of developing PD. Such variations may be found in genes implicated in familial PD (*6*, *23*) or in genes in signaling pathways that have not yet been implicated in PD (*3*, *24*). The accumulation of genetic variants associated with PD may also explain the high incidence of shared clinical syndromes in family members who do not share the familial genetic mutation (*25*).

Here, we generate neural cells from induced pluripotent stem cells (iPSCs) derived from fibroblasts from familial PD patients carrying

[1]Neuroregeneration Institute, McLean Hospital/Harvard Medical School, Belmont, MA 02478, USA. [2]Neuroregeneration and Stem Cell Programs, Institute for Cell Engineering, and Departments of Neurology and Neuroscience, Johns Hopkins University School of Medicine, Baltimore, MD 21205, USA. [3]Departments of Neurology, Psychiatry, and Pathology and Cell Biology, Sergievsky Center, Taub Institute and the Center for Motor Neuron Biology and Disease, Columbia University, New York, NY 10032, USA. [4]MassGeneral Institute for Neurodegenerative Disease, Massachusetts General Hospital, Harvard Medical School, Charlestown, MA 02129, USA. [5]Department of Physiology, Feinberg School of Medicine, Northwestern University, Chicago, IL, 60611, USA. [6]Department of Pathology and Laboratory Medicine, Institute on Aging and Center for Neurodegenerative Disease Research, University of Pennsylvania School of Medicine, Philadelphia, PA 19104, USA. [7]Department of Physiology and Biophysics, State University of New York at Buffalo, Buffalo, NY 14214, USA. [8]Departments of Neurology and Neuroscience, Mayo Clinic, Jacksonville, FL 32224, USA. [9]University of Florida Shands, Jacksonville, FL 32209, USA. [10]Department of Neurology, Medical University of Silesia, Katowice 40-055, Poland. [11]Section of Clinical and Molecular Neurogenetics at the Department of Neurology, University of Luebeck, 23562 Luebeck, Germany.
*These authors contributed equally to this work.
†NINDS PD iPS Cell Research Consortium.
‡Present address: Department of Molecular and Life Sciences, Hanyang University, Ansan 426-791, South Korea.
§To whom correspondence should be addressed. E-mail: isacson@hms.harvard.edu

the recessive homozygous Q456X mutation in *PINK1*, the dominant homozygous G2019S mutation in *LRRK2*, and the heterozygous R1441C substitution in *LRRK2*. iPSC-derived neural cells were also generated from fibroblasts from presymptomatic individuals and from healthy subjects not carrying these mutations. In parallel experiments performed in several collaborating laboratories, mitochondrial, proteasomal, and lysosomal function was analyzed in the iPSC-derived neural cells. The results of these assays were then used to characterize resulting neural cell phenotypes from individuals with genetically distinct forms of PD or without a family history of PD.

RESULTS

PINK1 and *LRRK2* mutations and vulnerability to chemical stressors

The phenotypic assays were performed at the same time in several laboratories using neural cells distributed from the same weekly batches of differentiated iPSC cultures. All iPSC clones were differentiated and analyzed in parallel. The iPSCs were generated from fibroblasts from three patients with familial PD, two asymptomatic individuals carrying PD-associated genetic mutations, and two healthy individuals who were not carrying genetic mutations associated with familial PD (figs. S1 to S3 and table S1). Comparative batch-batch analysis of iPSC differentiation confirmed the reproducibility of the broad neural cell types used for the phenotypic assays (fig. S4). The populations of neural cells contained DA neurons, non-DA neurons, and immature cells of these lineages. Neural cell vulnerabilities to PD-associated chemical toxins and stressors targeting either mitochondrial function or protein degradation (Fig. 1) were determined in parallel by measuring cellular release of lactate dehydrogenase (LDH) and intracellular activity of MTS [reductase 3-(4,5-dimethylthiazol-2-yl)-5-(3-carboxymethoxyphenyl)-2-(4-sulfophenyl)-2*H*-tetrazolium]. Because the LDH and MTS assays produced similar dose responses, only the data from the LDH assays are shown (Table 1). The genotype-specific cytotoxicity profiles showed that neural cells from patients with the *PINK1* Q456X mutation were more vulnerable to valinomycin (0.5 to 100 μM), MPP^+ (1-methyl-4-phenylpyridinium) (0.05 and 5 μM), concanamycin A (10 to 100 nM), hydrogen peroxide (1 to 10 μM), and MG132 (carbobenzoxy-L-leucyl-L-leucyl-L-leucinal) (1 μM) than those from healthy subjects (fig. S5). Neural cells from individuals carrying *LRRK2* mutations shared a vulnerability to valinomycin (0.5 to 100 μM), concanamycin A (10 and 50 nM), and MPP^+ (0.05 μM) (fig. S6). From analyses using the same batches of cells as used in the LDH and MTS assays, immunocytochemistry and cell counts revealed fewer DA neurons among the neural cells from individuals carrying *PINK1* Q456X and *LRRK2* R1441C mutations compared to those from healthy subjects not carrying the genetic mutations after exposure to low concentrations of valinomycin and concanamycin A (table S4). These data show that iPSC-derived neural cells from patients with genetically distinct forms of PD or at-risk individuals share common vulnerabilities to valinomycin and concanamycin A. Furthermore, the data demonstrate the differential vulnerability of human neural cells, neurons, and DA neurons carrying PD-associated genetic mutations to valinomycin and concanamycin A.

Increased mROS in vulnerable PD PINK1 neural cells

Given that mitochondrial reactive oxygen species (mROS) are a primary source of cellular stress that can be induced by a wide variety of chemical stimuli, we examined whether low concentrations of chemical stressors such as the potassium ionophore valinomycin could increase mROS concentrations in neural cells from PD patients compared to healthy subjects. There was an increase in the production of mROS by neural cells from PD patients with *PINK1* mutations [0.1 μM valinomycin; 308.99 ± 101% SEM; $P < 0.05$, analysis of variance (ANOVA)] compared to healthy controls who did not carry familial PD-associated genetic mutations (0.1 μM valinomycin; 122.84 ± 7.16% SEM) in response to a low concentration of valinomycin (Fig. 2, A and B). Neural cells from PD patients and healthy subjects showed similar dose-dependent increases in mROS levels in response to low concentrations of hydrogen peroxide (Fig. 2C); the remaining chemical stressors did not change mROS levels in neural cells from either patients or healthy subjects (table S3).

The reduced form of glutathione (GSH) is an antioxidant that is important for preventing the damage caused by an increase in mROS concentrations. Given the combined cytotoxicity and increased mROS concentrations in neural cells from PD patients with the *PINK1* Q456X mutation in response to valinomycin, we next determined GSH concentrations in neural cells from *PINK1* Q456X patients and healthy subjects after exposure to low concentrations of valinomycin, concanamycin A, MPP^+, and hydrogen peroxide. Neural cells from *PINK1* Q456X patients contained reduced GSH after administration of low concentrations of valinomycin (1 and 10 μM), concanamycin A (10 nM), MPP^+ (5 μM), and hydrogen peroxide (10 μM) but not MG132 or

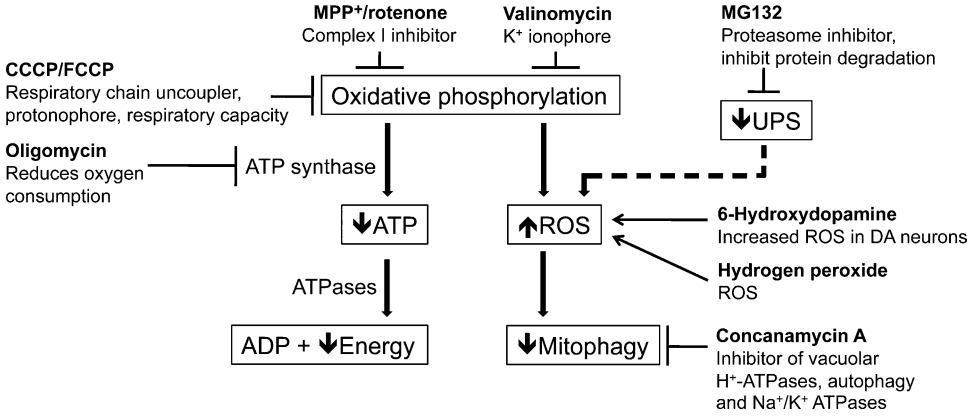

Fig. 1. Cellular stressors used to treat iPSC-derived neural cells from PD patients. To analyze cellular vulnerability and dysfunctional oxidative phosphorylation relevant to PD, we administered 10 different cellular stressors to iPSC-derived neural cells generated from familial PD patients and asymptomatic individuals carrying *PINK1* or *LRRK2* genetic mutations, and from healthy subjects who were not carrying these PD-associated mutations. The cellular stressors were known to affect pathways implicated in PD pathogenesis, such as oxidative phosphorylation, the autophagy-lysosomal pathway, or the ubiquitin-proteasome system (UPS).

Table 1. Sensitivity of iPSC-derived neural cells from PD patients and healthy subjects in response to chemical stressors (mean ± SEM of LDH release expressed as percent of Triton X-100 control; $n = 3$).

Neural cell genotype	Cellular stressor						
	Valinomycin (10 μM)	MPP^+ (5 μM)	Concanamycin A (10 nM)	Hydrogen peroxide (1 μM)	MG132 (1 μM)	CCCP (10 μM)	6-OHDA (10 μM)
Healthy subjects	30.1 ± 2.8	34.5 ± 2.2	39.3 ± 3.4	40.3 ± 2.8	35.1 ± 3.1	42.3 ± 4.1	31.4 ± 3.4
PINK1 Q456X homozygotes	52.3 ± 3.3*	41.4 ± 2.8*	51.6 ± 4.1*	52.3 ± 4.1*	44.5 ± 4.8*	48.2 ± 4.4	33.1 ± 2.7
LRRK2 G2019S homozygote	42.8 ± 3.9*	39.5 ± 4.2	48.4 ± 3.9*	49.3 ± 8.2	38.5 ± 4.9	52.4 ± 6.3	34.5 ± 4.1
LRRK2 R1441C heterozygotes	45.3 ± 3.9*	37.5 ± 5.2	53.7 ± 4.5*	48.2 ± 7.3	40.4 ± 3.9	53.1 ± 5.7	35.7 ± 3.1

*$P < 0.05$, ANOVA.

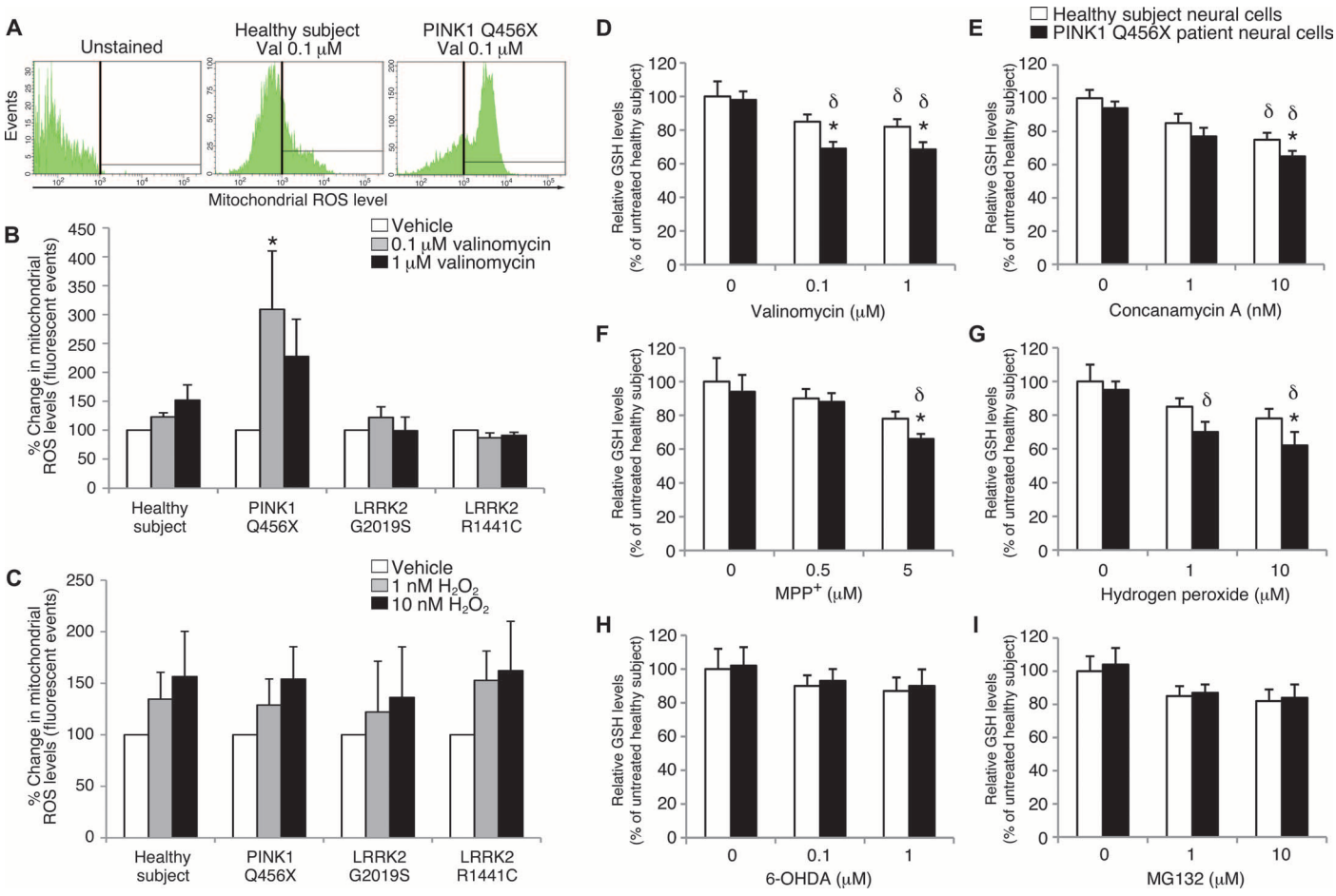

Fig. 2. Effects of cellular stressors on iPSC-derived neural cells with a *PINK1* mutation. iPSC-derived neural cells from PD patients carrying the *PINK1* Q456X homozygous mutation were treated with low concentrations of valinomycin, and then mROS and GSH concentrations were measured. (**A** to **C**) After 24 hours of incubation in vehicle and 0.1 or 1 μM valinomycin, patient-specific neural cells were labeled with a fluorescence indicator of mROS and analyzed by fluorescence-activated cell sorting. (A) Few fluorescent cellular events were recorded from healthy subject neural cells exposed to 0.1 μM valinomycin relative to unstained cultures. In contrast, many fluorescent cellular events representing increased mROS production were recorded from *PINK1* patient neural cells exposed to 0.1 μM valinomycin. (B) Quantification of fluorescent events revealed that 0.1 μM valinomycin increased the percentage of fluorescent *PINK1* patient-specific neural cells. (C) Parallel incubations of healthy subject and patient-specific neural cells with 1 or 10 nM hydrogen peroxide (H_2O_2) showed dose-dependent increases in the percentage of fluorescent cellular events independent of genotype, confirming the specificity of the assay for mROS. (**D** to **I**) After exposure to valinomycin (0.1 or 1 μM) (D), concanamycin A (10 nM) (E), MPP^+ (5 μM) (F), or H_2O_2 (10 μM) (G), *PINK1* patient neural cells (black bars) showed reduced GSH levels relative to healthy control neural cells (white bars). In contrast, low concentrations of 6-OHDA (1 or 10 μM) (H) or MG132 (1 or 10 μM) (I) did not change GSH levels in *PINK1* patient or healthy subject neural cells. Data are represented as means ± SEM. $n = 3$. *$P < 0.05$, ANOVA, *PINK1* PD patients versus healthy subjects; $^{\delta}P < 0.05$, ANOVA, chemical stressor versus vehicle.

6-hydroxydopamine (6-OHDA) (Fig. 2, D to I). Together, the cytotoxicity profiles and the changes in mROS and GSH concentrations suggest that iPSC-derived neural cells from PD patients carrying the *PINK1* mutation show increased vulnerability to cellular oxidative stress compared to neural cells from healthy individuals.

Mitochondrial respiration in neural cells from individuals carrying *PINK1* or *LRRK2* mutations

Next, we determined the rates of oxygen consumption by neural cells derived from individuals carrying PD-associated genetic mutations in *PINK1* or *LRRK2* and healthy subjects without these genetic mutations in response to the adenosine triphosphate (ATP) synthase inhibitor oligomycin (antibiotic), the proton ionophore FCCP (carbonyl cyanide *p*-trifluoromethoxyphenylhydrazone), and the mitochondrial complex I inhibitor rotenone (pesticide) (Fig. 3). The basal oxygen consumption rate (OCR) of neural cells from PD patients with *PINK1* mutations was greater than that for healthy subjects; exposure to oligomycin did not reduce the OCR (Fig. 3, A and B). Neural cells from both PD patients with *PINK1* mutations and healthy subjects showed similar responses in OCR to FCCP and rotenone. Furthermore, neural cells from *PINK1* PD patients showed an increased difference between oligomycin- and rotenone-mediated inhibition of OCRs. This represented energy substrate (ATP)–independent respiration and an increase in the passive leak of protons from the inner mitochondrial membrane (Fig. 3C). The results from the full experiment (Fig. 3, T.M.D. lab) were confirmed in a parallel exploratory experiment using the same neural cells but adding oligomycin, CCCP (carbonyl cyanide 3-chlorophenylhydrazone), and the electron transport chain inhibitor antimycin A to the neural cell culture medium (fig. S7, D.K. lab).

The basal OCRs of iPSC-derived neural cells from individuals carrying the *LRRK2* G2019S and R1441C mutations were reduced compared to iPSC-derived neural cells from healthy subjects (Fig. 3, D, E, G, and H). The neural cells from individuals carrying *LRRK2* G2019S and R1441C mutations and healthy subjects showed similar changes in OCRs in response to oligomycin, FCCP, and rotenone (Fig. 3, D, E, G, and H). Furthermore, the similar levels of oligomycin and rotenone inhibition of OCRs indicated that proton leakage was not increased in neural cells from individuals carrying either *LRRK2* G2019S or R1441C mutations (Fig. 3, F and I). The shared profiles of mitochondrial dysfunction among iPSC-derived neural cells from individuals carrying different PD-associated genetic mutations suggest a common vulnerability to altered cellular bioenergetics.

Dysfunctional mitochondrial mobility in PD *LRRK2* mutant neurons

Mitochondrial transport allows cells to respond to regional changes in metabolism and protect their mitochondria from damage. To discern the consequences of PD-associated genetic mutations on mitochondrial biology, we examined mitochondrial dynamics in iPSC-derived neurons from individuals carrying *LRRK2* and *PINK1* genetic mutations and healthy subjects using live-cell imaging. Mitochondria in the proximal axon of neurons from individuals carrying the *LRRK2* G2019S mutation (72.4 ± 4.6% SD) and R1441C mutation (61.1 ± 3.8% SD) were more mobile (percentage of mitochondria moving in any direction during the 5-min recording) than similarly located mitochondria in neurons derived from healthy subjects (47.25 ± 1.6% SD; $P < 0.05$, ANOVA; Fig. 4A). The mobility of mitochondria in neurons from PD patients with the *PINK1* Q456X mutation was similar to mitochondrial movement in neurons from healthy subjects (Fig. 4A).

Regarding the direction of movement, mitochondria in the proximal axon of neurons from PD patients with the *LRRK2* G2019S mutation showed more bidirectional (nonmonotonic) movement (percentage of mitochondria moving in both directions, anterograde and retrograde, 21.7 ± 5.1% SD) than mitochondria in neurons from healthy subjects (8.60 ± 1.07% SD; $P < 0.05$, ANOVA; Fig. 4, A and D). An increase in bidirectional mobility of mitochondria in neurons from *LRRK2* G2019S PD patients was also found.

The length of axons (that is, long, thin processes with uniform diameters) did not differ between neurons from healthy subjects (30.7 ± 16.2 μm SD, $n = 88$, by Kolmogorov-Smirnov test) and neurons from individuals carrying PD-associated genetic mutations (*PINK1* Q456X: 33.5 ± 17.5 μm SD, $n = 81$; *LRRK2* R1441C: 33 ± 12.1 μm SD, $n = 51$; *LRRK2* G2019S: 31.3 ± 10.8 μm SD, $n = 25$; Fig. 4B). As for the length of each mitochondrion in the axons, mitochondria in the proximal axon of neurons from individuals carrying the *LRRK2* R1441C mutation (1.8 ± 1.0 μm SD, $n = 283$; $P = 0.041$ by Kolmogorov-Smirnov test) were found to be 20% shorter than those in axons of neurons derived from healthy subjects (2.25 ± 1.36 μm SD, $n = 430$; Fig. 4, C and E). Mitochondria in neurons from *PINK1* Q456X PD patients (2.34 ± 2.81 μm SD, $n = 463$) or *LRRK2* G2019S PD patients (1.91 ± 0.86 μm SD, $n = 116$) were similar in length to neuronal mitochondria from healthy subjects. These findings suggest that the *LRRK2* mutations in PD patient–specific neurons are associated with altered mitochondrial dynamics and morphology.

Pharmacological rescue of PD patient neural cell vulnerability

Cytotoxicity assays demonstrated that iPSC-derived neural cells from individuals carrying *PINK1* and *LRRK2* mutations are more vulnerable to the chemical toxins valinomycin and concanamycin A than those from healthy subjects. To examine whether this cellular vulnerability could be reduced pharmacologically, we treated iPSC-derived neural cells carrying *PINK1* and *LRRK2* genetic mutations with the antioxidant coenzyme Q_{10} or rapamycin or the LRRK2 inhibitor GW5074 during exposure to low concentrations of either valinomycin or concanamycin A. Measurements of LDH release demonstrated that treatment with coenzyme Q_{10} reduced the vulnerability of iPSC-derived neural cells with *PINK1* Q456X, *LRRK2* G2019S, and *LRRK2* R1441C mutations to the lowest concentration of valinomycin (0.1 μM; Fig. 5, A, C, and E) and concanamycin A (1 nM; Fig. 5, B, D, and F). However, coenzyme Q_{10} did not reduce LDH release by the same iPSC-derived neural cells in response to higher concentrations of valinomycin (1 μM) and concanamycin A (10 nM). Although rapamycin reduced LDH release from *LRRK2* mutant neural cells exposed to valinomycin but not concanamycin A, neural cells from PD patients with *PINK1* mutations were unresponsive to rapamycin (Fig. 5, A and B). Treatment with the LRRK2 inhibitor GW5074 reduced LDH release from neural cells from *PINK1* Q456X PD patients exposed to valinomycin but not to concanamycin A (Fig. 5, A and B). GW5074 also reduced LDH release from neural cells with *LRRK2* mutations in response to both valinomycin and concanamycin A (Fig. 5, C to F). Next, we examined whether the induction of mROS production in *PINK1* PD patient neural cells in response to a low concentration of valinomycin could be reduced pharmacologically. Neural cells from *PINK1* Q456X PD patients or healthy

subjects were administered coenzyme Q_{10}, rapamycin, or GW5074 during exposure to valinomycin. Neither coenzyme Q_{10}, rapamycin, nor GW5074 affected mROS production in neural cells from healthy subjects (fig. S8A). In contrast, both rapamycin and GW5074 reduced mROS production by *PINK1* PD patient neural cells exposed to 0.1 μM valinomycin (fig. S8B).

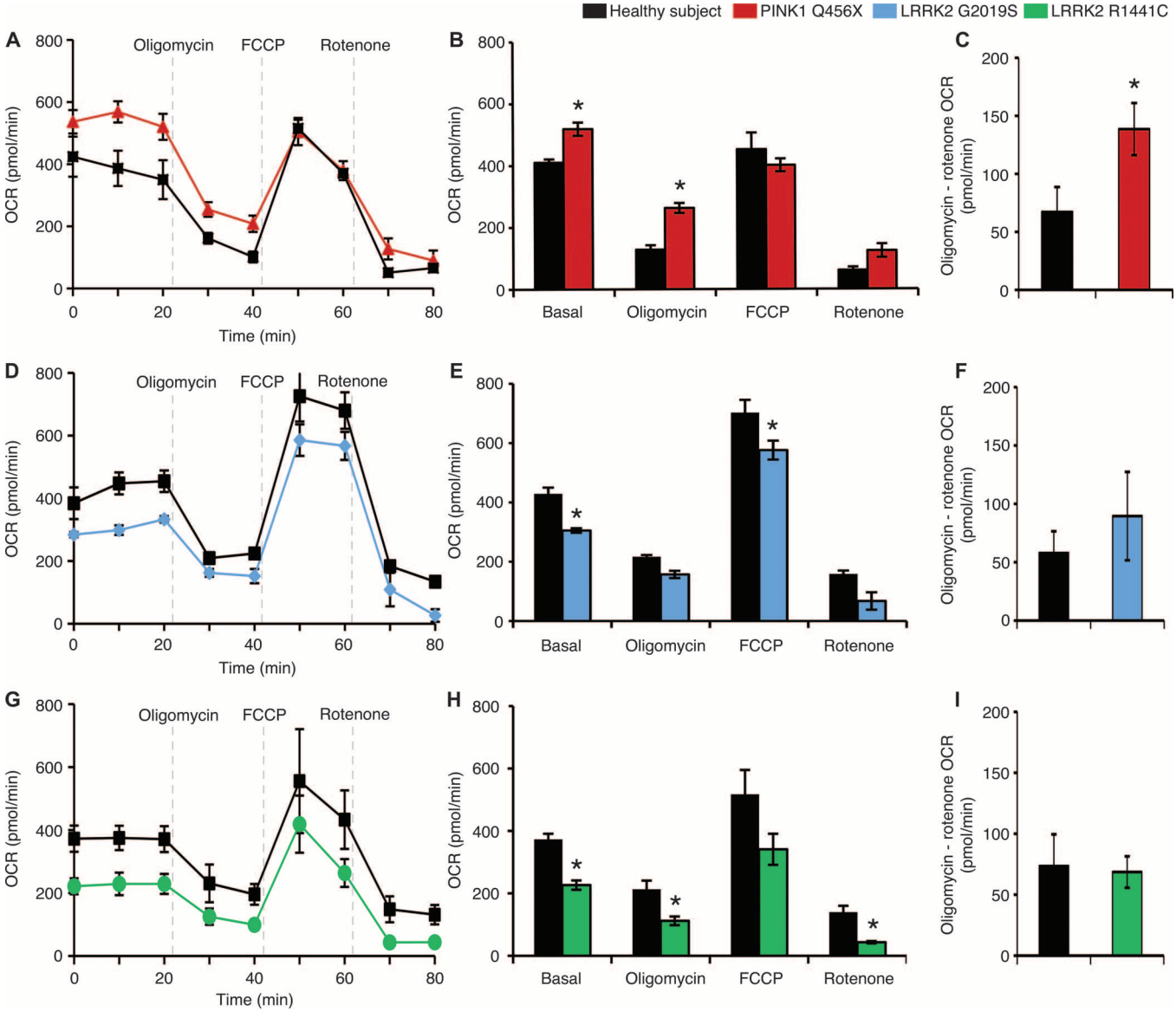

Fig. 3. Respiration in PD patient iPSC-derived neural cells. (**A**) iPSC-derived neural cells from healthy subjects (black) or PD patients carrying the *PINK1* Q456X mutation (red) were administered oligomycin (which inhibits ATP synthesis), FCCP (which induces maximum respiratory capacity), and rotenone (which inhibits total mitochondrial respiration) sequentially, and the OCR, indicative of oxidative phosphorylation, was measured in real time. (**B**) Quantification of the OCR for each cellular stressor demonstrated an increased basal respiration rate and reduced sensitivity to oligomycin of *PINK1* Q456X patient neural cells. (**C**) Subtraction of the rotenone-induced OCR from the oligomycin OCR demonstrated an increase in proton leakage from *PINK1* Q456X PD patient neural cells. (**D**) iPSC-derived neural cells from healthy subjects (black) and from a PD patient carrying the *LRRK2* G2019S mutation (blue) were treated with oligomycin, FCCP, and rotenone sequentially, and the OCR was measured in real time. (**E**) iPSC-derived neural cells from a PD patient carrying the *LRRK2* G2019S mutation exhibited a reduced basal respiration rate and increased sensitivity to FCCP. (**F**) Subtraction of the rotenone-induced OCR from the oligomycin OCR demonstrated that the levels of proton leakage from *LRRK2* G2019S patient neural cells were similar to those for healthy subject neural cells. (**G**) iPSC-derived neural cells from healthy subjects (black) or individuals carrying the *LRRK2* R1441C mutation (green) were administered oligomycin, FCCP, and rotenone sequentially, and the OCR was measured in real time. (**H**) *LRRK2* R1441C patient neural cells exhibited a reduced basal respiration rate and increased sensitivity to both oligomycin and rotenone. (**I**) Subtraction of the rotenone-induced OCR from the oligomycin OCR demonstrated that the levels of proton leakage from *LRRK2* R1441C patient neural cells were similar to those for healthy subject neural cells. Data are represented as means ± SEM. $n = 3$. *$P < 0.05$, ANOVA.

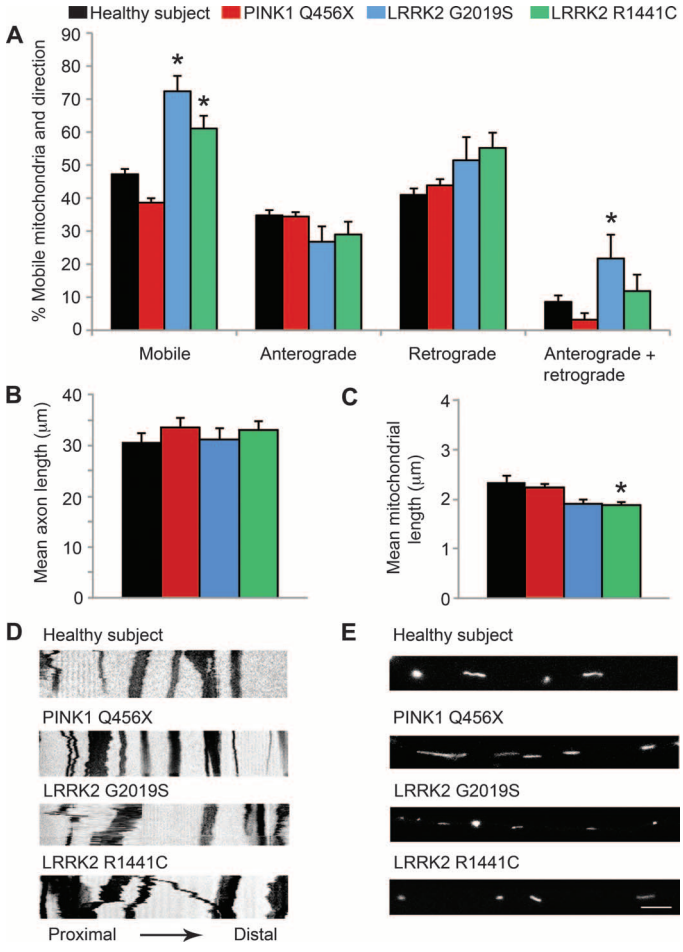

Fig. 4. Mobility of mitochondria in the proximal axon of iPSC-derived neurons from PD patients. (**A**) Live-cell imaging showed that the mitochondria in the proximal axons of neurons from individuals carrying *LRRK2* G2019S and R1441C mutations moved more randomly than similarly located mitochondria in healthy control neurons. Further analysis showed that mitochondrial movements in the proximal axons of *LRRK2* G2019S patient neurons were more bidirectional (both anterograde and retrograde movement) than those in healthy control neurons. *$P < 0.05$, ANOVA. (**B**) The axons of neurons from healthy subjects and individuals carrying *PINK1* Q456X, *LRRK2* G2019S, and *LRRK2* R1441C mutations were the same length (Kolmogorov-Smirnov test). (**C**) However, the mitochondria in neurons from individuals carrying the *LRRK2* R1441C mutation were shorter than those in healthy control neurons. *$P < 0.05$, Kolmogorov-Smirnov test. (**D**) Representative kymographs of mitochondria labeled with mitoDendra fluorescent protein in proximal axons of neurons from healthy subjects and from individuals carrying *PINK1* Q456X, *LRRK2* G2019S, and *LRRK2* R1441C mutations were taken every 5 s for 5 min. (**E**) Representative images are shown for mitochondria labeled with mitoDendra fluorescent protein in the proximal axons of neurons from healthy subjects and from individuals carrying *PINK1* Q456X, *LRRK2* G2019S, and *LRRK2* R1441C mutations. Data are represented as means ± SD. $n = 3$.

PINK1 and *LRRK2* PD neural cells are more sensitive to chemical stressors than fibroblasts

Finally, we examined whether cellular reprogramming is required for the cytotoxicity phenotypes observed in neural cells from individuals carrying *LRRK2* and *PINK1* genetic mutations. LDH release in response to a full range of valinomycin and concanamycin A concentrations was measured for iPSC-derived neural cells and for fibroblasts taken directly from familial PD patients (Fig. 6). Exposure to valinomycin caused both *PINK1* PD patient neural cells (Fig. 6A) and fibroblasts (Fig. 6B) to release more LDH than iPSC-derived neural cells or fibroblasts from healthy subjects. Greater concentrations of valinomycin were required to induce vulnerability to oxidative stress in fibroblasts compared to neural cells from *PINK1* PD patients. In response to concanamycin A, *PINK1* PD patient neural cells released more LDH than those from healthy subjects (Fig. 6C), but *PINK1* PD patient and healthy control fibroblasts released similar levels of LDH (Fig. 6D). Similar results were obtained for iPSC-derived neural cells and fibroblasts from PD patients with the *LRRK2* G2019S and R1441C mutations in response to valinomycin and concanamycin A (Fig. 6, E to H). In response to valinomycin, iPSC-derived neural cells carrying *LRRK2* mutations released more LDH than those from healthy subjects (Fig. 6E), but *LRRK2* PD patient fibroblasts did not release more LDH than those from healthy subjects (Fig. 6F). In response to concanamycin A, neural cells (Fig. 6G) and fibroblasts (Fig. 6H) from individuals carrying either of the *LRRK2* mutations released more LDH than neural cells and fibroblasts from healthy subjects. *LRRK2* PD patient fibroblasts released less LDH than iPSC-derived neural cells with *LRRK2* mutations when treated with either valinomycin or concanamycin A (Fig. 6, E to H).

DISCUSSION

We first focused on determining phenotypes for iPSC-derived neural cells generated from patients with familial forms of PD and at-risk individuals. Our rationale was based on the fact that patients with sporadic forms of PD share many of the symptoms of patients carrying *PINK1* and *LRRK2* mutations. The disease in patients with sporadic forms of PD is less well defined because it may be caused by a combination of cumulative genetic variants and greater environmental effects than is the case with familial forms of PD. We therefore decided to first examine mitochondrial dysfunction in iPSC-derived neural cells from patients with rare familial forms of PD to see whether there are commonalities in terms of vulnerabilities to chemical stressors and toxins (*26*). It is hoped that future experiments using iPSC-derived neural cells from patients with sporadic PD may show some of the same phenotypic features identified in iPSC-derived neural cells from PD patients with *PINK1* and *LRRK2* mutations.

In our experiments, we observed an increase in sensitivity to chemical stressors as the cell type analyzed became functionally closer to the vulnerable cell types in the PD brain, that is, an increase in sensitivity in iPSC-derived neural cells and neurons compared to fibroblasts from the same patient. The iPSC-derived neural cells from the different PD-associated genotypes shared similar vulnerabilities to chemicals such as valinomycin that induced mitochondrial depolarization with K^+ ions (*27*–*29*). In contrast, the iPSC-derived neural cells from PD patients were not vulnerable to CCCP, which depolarizes mitochondria using protons (H^+) (*30*). Compared to healthy control neural cells, PD patient neural cells also showed increased sensitivity to concanamycin A, a specific inhibitor of vacuolar-type H^+-dependent adenosine triphosphatases (V-ATPases) that regulate autophagy and membrane transport (*31*, *32*). However, a similar inhibitor of V-ATPases can change

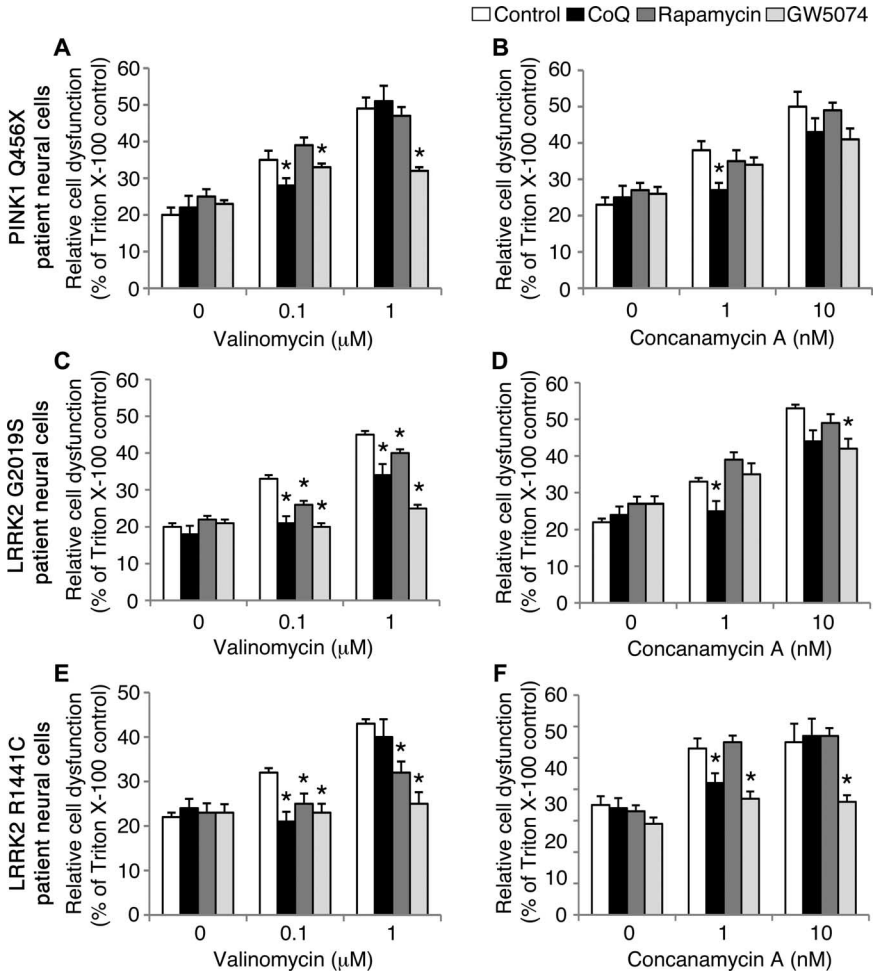

Fig. 5. Pharmacological treatment of iPSC-derived neural cells from PD patients. iPSC-derived neural cells from individuals with *PINK1* and *LRRK2* mutations were treated with coenzyme Q_{10}, rapamycin, or GW5074 after exposure to low doses of valinomycin or concanamycin A, and then LDH release was measured. (**A** to **F**) The administration of either valinomycin (0.1 and 1 μM) or concanamycin A (1 and 10 nM) increased LDH release from *PINK1* Q456X, *LRRK2* G2019S, and *LRRK2* R1441C PD patient neural cells (white bars). (A) Treatment with 1 μM coenzyme Q_{10} (CoQ) (black bars) or 1 μM GW5074 (light gray bars) but not 1 μM rapamycin (dark gray bars) reduced LDH release by *PINK1* PD patient neural cells induced by valinomycin (control, white bars). (B) Treatment with coenzyme Q_{10} but not rapamycin or GW5074 reduced LDH release from *PINK1* Q456X PD patient neural cells induced by concanamycin A (control, white bars). (C) Treatment with coenzyme Q_{10}, rapamycin, or GW5074 reduced LDH release by *LRRK2* G2019S PD patient neural cells induced by valinomycin (control, white bars). (D) Treatment with coenzyme Q_{10} or GW5074 but not rapamycin reduced LDH release by *LRRK2* G2019S PD patient neural cells induced by concanamycin A (control, white bars). (E) Treatment with coenzyme Q_{10}, rapamycin, or GW5074 reduced LDH release by neural cells from individuals carrying the *LRRK2* R1441C mutation induced by valinomycin (control, white bars). (F) Treatment with coenzyme Q_{10} or GW5074 but not rapamycin reduced LDH release by neural cells from individuals carrying the *LRRK2* R1441C mutation induced by concanamycin A (control, white bars). The relative cell dysfunction was calculated from LDH release values as a percentage of untreated cells completely lysed by incubation with Triton X-100. Data are represented as means ± SEM. $n = 3$. *$P < 0.05$, ANOVA.

mitochondrial respiration and exhibits K^+ ionophore activity (*33*, *34*). Given the shared vulnerability of *PINK1* and *LRRK2* PD patient neural cells to valinomycin and concanamycin A but not CCCP, it is possible that the PD-associated mutations compromised the ability of the iPSC-derived neural cells to efficiently respond to mitochondria damaged by the influx of K^+ ions. Measuring cellular vulnerabilities to direct ROS (H_2O_2), induced mROS and other stressors indicated that the iPSC-derived neural cells from *PINK1* Q456X patients were less able to respond to oxidative stress. The findings suggest that iPSC-derived neural cells from PD patients carrying *PINK1* mutations may use mitochondrial proton leakage to minimize oxidative damage due to loss of PINK1 activity (*27*, *35*, *36*). In contrast, the OCRs show that the mitochondrial electron transport chain is intact in PD patient neural cells carrying *LRRK2* mutations, but the reduced levels of basal respiration in these cells suggest that the increased kinase activity caused by the *LRRK2* mutations reduces the availability of substrates for oxidative phosphorylation (*37*). The *LRRK2* mutations were also associated with disrupted mitochondrial movement in PD patient–specific neurons. Dysfunctional axonal trafficking has been implicated in PD as an early event that precedes neurodegeneration (*38*–*40*). LRRK2 regulates the stability of neuronal microtubules that are required for efficient trafficking of mitochondria to energy-dependent regions within neurons (*41*, *42*). The combination of altered mitochondrial dynamics and reduced basal respiration in LRRK2 PD patient neural cells may contribute to the vulnerability of these neurons in PD.

The pharmacological rescue of the genotype-specific vulnerabilities to valinomycin and concanamycin A also provided some mechanistic insight. The rescue of *PINK1* Q456X PD patient neural cells from low concentrations of valinomycin and concanamycin A by the antioxidant coenzyme Q_{10} and the LRRK2 inhibitor GW5074 is consistent with the hypothesis that loss of PINK1 leads to production of ROS through an LRRK2-associated mechanism (*15*, *43*, *44*). Rapamycin inhibits the activity of the mammalian target of rapamycin (mTOR) and can improve lysosomal degradation and activate the prosurvival signaling molecule AKT in PD cellular and animal models (*45*–*47*). In our experiments, rapamycin did not protect *PINK1* Q456X PD patient neural cells from either valinomycin or concanamycin A. This contrasts with the neuroprotective effects of rapamycin observed in *Drosophila* carrying a *PINK1* null mutation (*48*). Rapamycin reduced the vulnerability of both *LRRK2* G2019S and R1441C PD patient neural cells to valinomycin, suggesting a potential link between *LRRK2*, mitochondrial dysfunction, lysosomal degradation, and AKT activation. The LRRK2 inhibitor GW5074 provided some protection against valinomycin- and concanamycin A–induced toxicity in both *LRRK2* G2019S and

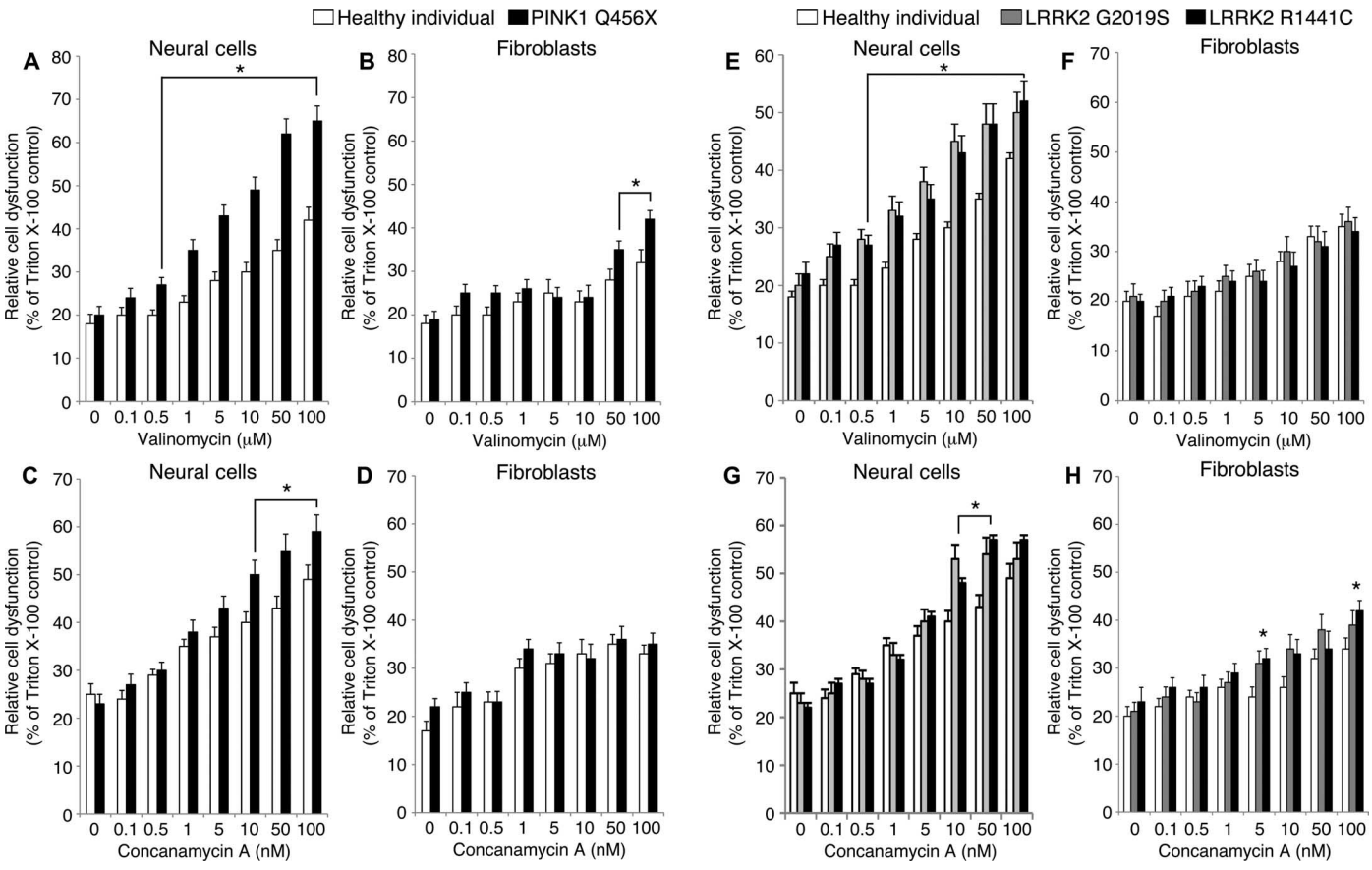

Fig. 6. Cell type–specific vulnerability to cellular stressors and oxidative stress. iPSC-derived neural cells from individuals carrying *PINK1* and *LRRK2* mutations are more vulnerable to both valinomycin and concanamycin A than primary fibroblasts taken from the same PD patients. (**A**) In response to a range of valinomycin concentrations, *PINK1* patient neural cells (white bars) released more LDH than healthy control neural cells (black bars). (**B**) Similarly, *PINK1* PD patient fibroblasts (white bars) released more LDH than fibroblasts from healthy subjects (black bars) in response to valinomycin, albeit at greater concentrations of valinomycin than *PINK1* PD patient neural cells. (**C**) In response to a range of concentrations of concanamycin A, *PINK1* PD patient neural cells (white bars) released more LDH than healthy subject neural cells (black bars). (**D**) In contrast, *PINK1* PD patient (white bars) and healthy subject (black bars) fibroblasts released similar amounts of LDH in response to concanamycin A. (**E**) In response to a range of concentrations of valinomycin, iPSC-derived neural cells from individuals carrying *LRRK2* G2019S (gray bars) and *LRRK2* R1441C (black bars) mutations released more LDH than healthy subject neural cells (white bars). (**F**) In contrast, *LRRK2* G2019S PD patient (gray bars), *LRRK2* R1441C PD patient (black bars), and healthy subject (white bars) fibroblasts released similar levels of LDH in response to valinomycin. (**G**) In response to a range of concentrations of concanamycin A, neural cells from individuals carrying the *LRRK2* G2019S mutation (gray bars) and *LRRK2* R1441C mutation (black bars) released more LDH than healthy subject neural cells (white bars). (**H**) Similarly, *LRRK2* G2019S PD patient fibroblasts (gray bars) and *LRRK2* R1441C PD patient fibroblasts (black bars) released more LDH than healthy subject fibroblasts (white bars) in response to concanamycin A, but the LDH levels were lower than for iPSC-derived neural cells from the same PD patients. The relative cell dysfunction was calculated from LDH release values as a percentage of untreated cells completely lysed by incubation with Triton X-100. Data are represented as means ± SEM. $n = 3$. *$P < 0.05$, ANOVA.

R1441C PD patient neural cells, consistent with a previous study showing that GW5074 protected mice against LRRK2-mediated toxicity (*15*).

Our findings raise several interesting points. First, the genotype-specific phenotypic profiles suggest possible shared cellular disease pathways for familial forms of PD. The broader range of neural cell vulnerabilities associated with the loss of *PINK1* expression compared to that of neural cells from individuals with *LRRK2* mutations is consistent with an increased genetic risk and an earlier age of onset of PD in patients carrying the *PINK1* Q456X mutation compared to either of the *LRRK2* mutations. The shared vulnerability to chemical stressors, and the similar respiratory and mitochondrial mobility profiles for both *LRRK2* G2019S and R1441C neural cells, suggests that both mutations cause similar downstream dysfunction.

Second, cell type–specific vulnerability, that is, preferential degeneration of nigrostriatal DA neurons, is a characteristic of PD. It has not been clear whether patient-specific iPSCs can provide populations of neural cells that can robustly model PD disease pathogenesis. Given that fibroblasts from PD patients carrying *PINK1* and *LRRK2* mutations exhibit phenotypes (*49*–*52*), it seems reasonable to suppose that iPSC-derived neural cells are a useful human cellular model for dissecting pathogenic events in PD. Our data demonstrate cell type–specific vulnerability because PD patient–specific neural cells differentiated from iPSCs were more sensitive to cellular stressors than fibroblasts carrying

similar mutations. Our data are consistent with the hypothesis of cell type–specific vulnerability developed for PD patients, where the midbrain DA neurons are more vulnerable than neighboring neuronal subtypes that also express genes associated with familial PD (*1*, *53*, *54*).

Third, in terms of using iPSCs to model PD pathogenesis, we think that the cell stress assays we have used provide an opportunity to investigate aspects of aging-related pathogenesis and the responses of individual PD patients to different treatments. For example, the age-related accumulation of dysfunctional mitochondria (*55*, *56*) can be mimicked using low doses of mitochondrial stressors, such as valinomycin or MPP^+, which create controlled, widespread mitochondrial damage within a cell population.

Cellular reprogramming technology has been proposed as a platform for predicting disease phenotypes and drug efficacy or to classify drug-responsive cohorts based on genetics (*57*–*59*). Even with advances in genomic sequencing and a better understanding of phenotypic-genotypic correlations performed on kindreds, the biological basis for predicting drug responses in familial or sporadic forms of PD is unclear. Our data from the dose responses of *PINK1* and *LRRK2* PD patient neural cells to coenzyme Q_{10}, rapamycin, and GW5074 suggest that cellular reprogramming technology may be able to help define patient cohorts that are responsive to different pharmacological treatments. For future clinical impact, it will be essential to determine cellular responses during the presymptomatic phase of the disease, when neuroprotective interventions are predicted to be most efficacious.

Our findings provide evidence of differences in responses to cellular stress for iPSC-derived neural cells from PD individuals carrying genetic mutations associated with different forms of familial disease. These data show that iPSC-derived neural cells are sensitive models for measuring vulnerability to chemical stressors and responses to candidate neuroprotective molecules. They may help to identify causes of PD and potential new drugs and treatments for PD.

MATERIALS AND METHODS

Clinical data for patient-specific iPSC lines

The iPSC lines were generated from seven subjects from three families with PD under informed consent. Subjects 1 (II:5) and 2 (II:7) were family members that share homozygous *PINK1* Q456X mutations (family W) (*21*). Briefly, the age of onset of the PD patients with *PINK1* Q456X mutations was 61 and 53 years and they had scores of 2 and 2.5 on the Hoehn and Yahr scale, respectively, indicating bilateral symptoms. Subjects 3 and 4 were 59-year-old Caucasian twins (sister and brother) from a family with PD (family D) (*9*, *60*). They each had a heterozygous *LRRK2* R1441C mutation inherited from their father who had PD. Neither of these subjects was clinically affected, but subject 3 (brother) showed some resting tremor. Subject 5 was a 78-year-old Caucasian man (family US1) whose age at onset was 55 years; he had a score of 3.5 on the Hoehn and Yahr scale, indicating moderate to severe disability. He carried a homozygous *LRRK2* G2019S mutation and his brother, maternal aunt, and paternal uncle had been diagnosed with PD [(*61*) and unpublished data]. His symptoms were responsive to anti-parkinsonism therapy. Subjects 6 and 7 were 59 and 40 years, respectively, at skin biopsy and were from the same family as subjects 1 and 2 but did not have a known PD-associated mutation and were clinically unaffected at the time of biopsy. Skin fibroblasts from each of the subjects were reprogrammed with standard methods (figs. S1 to S3 and table S1) (*27*, *62*), and the genotype was confirmed for each iPSC clone. The *LRRK2* G2019S genotype was confirmed by polymerase chain reaction–restriction fragment length polymorphism (PCR-RFLP) with Sfc I using *LRRK2* exon 31 genomic DNA as a template. The PCR product from homozygous *LRRK2* G2019S iPSCs was digested to produce 218– and 40–base pair (bp) fragments. The PCR product from human embryonic stem (ES) cells incubated with Sfc I produced a 258-bp band, consistent with nondigested DNA without the mutation. The *LRRK2* R1441C genotype was confirmed by PCR-RFLP with Bst UI using *LRRK2* exon 31 genomic DNA template. The 386-bp PCR product from human ES cells, with Arg at amino acid position 1441, was digested to produce 316- and 70-bp fragments (no mutation). In parallel, PCR products from *LRRK2* R1441C iPSCs were digested to produce bands at 386, 316, and 70 bp, consistent with a heterozygous mutation. In parallel genetic analyses, we confirmed that the patients' and at-risk individuals' iPSC lines did not carry additional major genetic mutations found in the other families of this study and the healthy subject iPSC lines did not carry *PINK1* Q456X, *LRRK2* G2019S, or *LRRK2* R1441C mutations.

Cellular reprogramming, validation, and differentiation

All iPSCs were generated with standard retrovirus-based protocols [(*62*, *63*) and see table S1]. Reverse transcription–PCR was performed as described (for primer sequences, see table S2). GTL banding of 20 metaphase cells per iPSC line confirmed normal karyotypes (Cell Line Genetics). Teratoma analyses were performed in nonobese diabetic/severe combined immunodeficient mice as described (*64*) (Applied StemCell). Genomic PCR (for genotyping primer sequences, see table S2) and direct sequencing of the products confirmed the genotypes of the iPSC lines with standard methods as described (*65*). The iPSCs were differentiated with standard protocols (*66*) except that recombinant human SHH-C24II protein was replaced by a small-molecule agonist of Smoothened (1 μM, Enzo) (*67*, *68*).

Patient fibroblast cell lines for determining cytotoxicity assays

For the fibroblast toxicity assays, we used the following PD patients' fibroblasts: two patients carrying *PINK1* mutations [*PINK1* Q456X homozygote (SC1028) and *PINK1* D525N/W577R compound (SC1027)], seven patients carrying *LRRK2* G2019S mutations (SC1007, SC1012, Coriell ID ND30623, ND29492, ND29542, ND29802, and ND30244), and two patients carrying *LRRK2* R1441C mutations (Coriell ID ND32386 PD2 and ND32944 PD3). Fibroblasts from two healthy subjects were used as controls (Coriell ID AG06010D and AG06959).

In vitro toxicity assays and pharmacological rescue of vulnerability

To assess the dose ranges for PD-associated toxins by LDH and MTS assays, we differentiated neural cells from all iPSC lines in parallel weekly batches (*66*). At 52 to 53 days in vitro, cells were plated on poly-L-ornithine (PLO)/laminin–coated 96-well plates at a density of 40,000 cells per well. Fibroblasts from PD patients or age-matched healthy subjects were plated on 96-well plates at a density of 5000 cells per well. Two days later, cells were incubated with valinomycin (0.1 to 100 μM, Sigma), concanamycin A (0.1 to 100 nM, Sigma), CCCP (0.1 to 100 μM, Sigma), hydrogen peroxide (0.01 to 10 μM, Fisher), 6-OHDA (0.1 to 100 μM, Sigma), MG132 (0.1 to 100 μM; Calbiochem), or MPP^+ (0.1 to 100 μM, Sigma) for 20 hours. Either water or dimethyl sulfoxide (DMSO) was used as vehicle and control conditions. The LDH and MTS assays were performed as described (*69*) (Roche). For the pharmacological rescue

experiments, a range of concentrations of coenzyme Q_{10} (Sigma), rapamycin (Sigma), or GW5074 (Tocris) was screened to minimize drug-mediated toxicity while reducing patient neural cell vulnerability to cellular stressors. The optimal dose of coenzyme Q_{10}, rapamycin, and GW5074 was determined to be 1 μM and was administered to the neural cells 30 min before and during exposure to the cellular stressors.

Determination of PD iPSC-derived neural cell OCRs

T.M.D. lab. Mitochondrial OCR in iPSC-derived neural cell cultures was analyzed in an XF24-3 Extracellular Flux Analyzer (Seahorse Bioscience). The OCR assay uses probes loaded on a sensor cartridge for fluorimetric detection of oxygen concentration. On day 53 of differentiation, cells were plated on V7 XF 24-well plates (Seahorse Bioscience) for 5 days. Four wells with no cells were set as background control for temperature-sensitive fluctuations in OCR analysis. For OCR measurements, culture medium was replaced with Seahorse XF medium supplemented with 25 mM glucose. The plates were preincubated in a CO_2-free incubator at 37°C for 30 min for equilibration and thereafter processed in the XF analyzer for OCR analysis. OCR analysis was initiated with a 20-min equilibration followed by three times cycles of 2-min mix, 2-min wait, and 2-min measurement time. All measurement cycles were performed at 37°C as described previously. Baseline OCR was recorded three times and followed by sequential injections of oligomycin (1 μM final concentration, Sigma), FCCP (3 μM final concentration, Sigma), and rotenone (1 μM final concentration, Sigma) into each well. The mix-wait-measure cycles were repeated two times after each drug injection. After the complete measurements of OCR analysis following the third drug injection (rotenone), the experiment was stopped and the data were transformed to show point-point mode display of OCR with background correction, using Seahorse XF software. The data were exported to Excel and normalized to cell number in each well. To determine cell numbers, we collected the medium containing detached cells in each well of XF plates in 1.5-ml tubes. TrypLE (200 μl) (Invitrogen) was added to each well of the plate. After incubation of the plate at 37°C for 3 min, the remaining cells from each well were pooled. The cells were centrifuged and the cell pellet was resuspended in phosphate-buffered saline and mixed with trypan blue (Invitrogen) for cell counting in an automated Countess Cell counting analyzer (Invitrogen).

D.K. lab. Mitochondrial OCR was determined by XF24 Extracellular Flux Analyzer (Seahorse Bioscience). Cells (60,000) were plated per well of XF24 plates. Four wells were left empty as background controls. On day 55 of differentiation, the OCR measurements were carried out in N2 medium added fresh on the morning of the experiment. Plates were preincubated in a CO_2-free incubator at 37°C for 30 min for equilibration before processing in the XF analyzer. For baseline measurements, a 20-min equilibration step was followed by five cycles of 2-min mix, 2-min wait, and 2-min measurement time. For analysis of drug response, three cycles of 2-min mix, 3-min wait, and 1.6-min measurement were used per condition. After three baseline measurements were taken, oligomycin (Sigma, 1 μM), CCCP (Sigma, 1 μM), and antimycin (Sigma, 0.1 μM) were added sequentially, with three measurements per condition. After the experiments, cells were harvested and DNA content was measured with Quant-iT PicoGreen (Invitrogen) to normalize for cell number. Data were plotted as absolute values (±SEM) to compare baseline OCR or as percent deviation from baseline (±SEM) after drug addition to compare the response to drugs between lines.

Flow cytometric detection of mitochondrial ROS in live PD iPSC-derived neural cells

For low-dose toxicity assays, neural cells differentiated from control or PD iPSC lines at 52 to 53 days in vitro were plated on 24-well PLO/laminin-coated plates at a density of 250,000 cells per well. Two days later, neural cells were incubated with toxins for 20 hours. mROS were identified by MitoSox (Invitrogen). Neural cells were dissociated with 0.05% trypsin, rinsed in Hanks' balanced salt solution (HBSS), and incubated in MitoSox working solution (50 μg MitoSox reconstituted in 13 μl of DMSO and diluted in 5 ml of warm HBSS) at a concentration of 250 μl per well of 24-well plate. The cells were incubated in MitoSox working solution at 37°C for 10 min in the dark. The cells were twice washed in warm HBSS before fluorescence-activated cell sorting analysis (FACSAria, BD Biosciences) at 510/580 nm with a live-cell gate and standard methods (*70*).

Immunocytochemistry and confocal microscopy

For immunocytochemistry, the primary antibodies were raised against tyrosine hydroxylase (TH) (Pel-Freez), type III β-tubulin (Covance), and FOXA2 (Santa Cruz Biotechnology). Indirect immunofluorescence and confocal microscopy were performed as described (*66*).

Determination of GSH levels

At 52 to 53 days in vitro of differentiation, 40,000 neural cells were plated per well of PLO/laminin-coated 96-well plates. Two days later, the neural cells were administered cellular stressors or vehicle for 24 hours and lysed. Following the manufacturer's protocol (GSH-Glo, Promega), the cell lysate was incubated with luciferin and glutathione *S*-transferase and intracellular GSH levels were measured by luminescence with a plate reader.

Live-cell imaging of mitochondrial dynamics

Live imaging experiments were performed in four-well chambered slides (Lab-Tek, Nunc). A pTurbo-mitoDendra expression vector (a gift from J. Magrane, Cornell University, New York) was used to visualize the mitochondria. Green fluorescent protein (GFP) was substituted with the Dendra coding region at the Age I and Not I sites of the pTurboGFP-mito (Evrogen). The construct was verified by sequencing. Cells were seeded (75,000 cells per chamber) onto PLO/laminin-coated surfaces (3 μg/ml each). Cells were maintained in Neurobasal complete medium, and only cells with a neuronal-like morphology (that is, multipolar cell bodies with at least two processes), which likely encompassed both neuronal progenitors and neurons, were selected for further analyses. Cells were transduced after 6 to 7 days in vitro with a pTurbo-mitoDendra–encoding lentivirus at various multiplicities of infection. Medium was changed after 12 hours, and live imaging was performed 72 hours later. Confocal microscopy was performed with a Nikon A1R MP confocal microscope (Nikon Instruments). The 488-nm laser was maintained below 0.5 mW to avoid photoconversion of Dendra. A 63× oil immersion objective and a pinhole measurement of ~2.5 Airy units (optical slice <2 μm) were used. Images were collected every 5 s for 5 min (61 frames). Only the proximal segment of the axon was acquired and recorded. Analyses of axonal and mitochondria lengths were performed as described (*71*). The dynamics of mitochondria along the axonal processes were studied with MetaMorph software (Universal Imaging). Kymographs were generated from each film (position versus time) and used to examine the fraction of mitochondria that were mobile with respect to those that were static. A mitochondrion was considered mobile if it changed its position in at least three consecutive frames. Within mobile mitochondria, we differentiated two different

populations: one monotonic (movement in one direction only) and one nonmonotonic (movement in various directions). Monotonic mitochondria are classified as anterograde and retrograde.

Electrophysiological recordings

Differentiated neural cell cultures were transferred to a recording chamber of an upright microscope equipped with a 40× water-immersion objective (Eclipse E600FN; Nikon) and perfused with saline containing 125 mM NaCl, 2.5 mM KCl, 25 mM $NaHCO_3$, 1.25 mM NaH_2PO_4, 2 mM $CaCl_2$, 1 mM $MgCl_2$, and 25 mM glucose (34°C; saturated with 95% O_2–5% CO_2; pH 7.4; 298 mosmol/liter). The saline flow rate was 2 to 3 ml/min running through an in-line heater (SH-27B with TC-324B controller; Warner Instruments). Neurons were visualized by video microscopy with a cooled charge-coupled device digital camera (CoolSNAP ES^2, Photometrics, Roper Scientific). Cells selected for electrophysiological recordings had neuron-like shapes showing distinguishable neurites. Somatic whole-cell patch-clamp recordings in current clamp configuration were performed with a MultiClamp 700B amplifier (Molecular Devices). Signals were filtered at 1 to 4 kHz and digitized at 5 to 20 kHz with a Digidata 1440A (Molecular Devices). Recording patch electrodes had a resistance of 4 to 6 megohms and were fabricated from filamented borosilicate glass (Sutter Instruments) pulled on a Flaming-Brown puller (P-97, Sutter Instruments). Patch electrodes were filled with internal solution containing 135 mM K-$MeSO_4$, 5 mM KCl, 5 mM Hepes, 0.25 mM EGTA, 10 mM phosphocreatine-di(tris), 2 mM ATP-Mg, and 0.5 mM guanosine triphosphate (GTP)–Na (pH 7.3, osmolarity adjusted to 290 to 300 mosmol/liter). For current-clamp recordings, the amplifier bridge circuit was adjusted to compensate for electrode resistance and monitored. Electrode capacitance was also compensated. If series resistance increased >20% during the recording, the data were discarded. To study the responsiveness of spontaneous active cells to current commands, we injected a holding current to hyperpolarize the membrane potential about −65 mV, avoiding the spontaneous firing. Then, step current commands were injected to elicit action potentials (1 s, 5 to 10 pA). Spontaneous activity was also recorded in current-clamp configuration without holding current.

Automated image acquisition and quantitative analysis of immunocytochemistry

Quantitative analysis of immunocytochemistry was performed on two coverslips per experimental condition. Each experimental condition was performed at least three times. Nine images per coverslip were acquired with an IN Cell Analyzer 2000 (GE Healthcare) at 20× magnification with autofocus. The exposure times were in the range of 0.02 to 0.03 s for Hoechst and β-tubulin and 0.07 to 0.1 s for TH (below saturation). Images were analyzed in an automatic, unbiased way with IN Cell Workstation Software (GE Healthcare). The numbers of all cells, β-tubulin–expressing neurons, and TH/β-tubulin–coexpressing cells were quantified with a multitarget analysis. Individual cells were identified as having a Hoechst-stained nuclear area larger than 25 μm^2 with top-hat segmentation. β-Tubulin– and TH-expressing cells were identified on the basis of respective staining in an area extending outside of the nucleus with a sensitivity setting of 50.

Statistical analysis

One- or two-way ANOVA with post hoc tests or Kolmogorov-Smirnov test was used to analyze the data (InStat, GraphPad Software Inc.; JMP, SAS Institute). $P < 0.05$ was considered significantly different.

SUPPLEMENTARY MATERIALS

www.sciencetranslationalmedicine.org/cgi/content/full/4/141/141ra90/DC1

Fig. S1. Cellular reprogramming of fibroblasts from a PD patient with a homozygous *LRRK2* G2019S mutation.

Fig. S2. Cellular reprogramming of fibroblasts from a PD patient with a heterozygous *LRRK2* R1441C mutation.

Fig. S3. Transgene silencing in iPSC lines.

Fig. S4. Categories of cell types differentiated from iPSC lines used in phenotypic assays.

Fig. S5. The vulnerability profile of *PINK1* Q456X homozygote patient-specific neural cells.

Fig. S6. The vulnerability profile of *LRRK2* patient-specific neural cells.

Fig. S7. Increased basal respiration and oxygen consumption of *PINK1* patient neural cells.

Fig. S8. Treatment with rapamycin or GW5074 reduces mROS levels in *PINK1* patient neural cells caused by a low dose of valinomycin.

Table S1. Patient genotypes and cellular reprogramming methods.

Table S2. PCR primer sequences (5′-3′).

Table S3. Healthy subjects' and PD patients' specific neural cell mROS levels in response to chemical stressors (mean ± SEM of % change in mitochondrial ROS levels).

Table S4. Healthy subjects' and PD patients' specific neural cell sensitivity to low concentrations of chemical stressors (mean ± SEM of % change in cell counts from vehicle-administered cultures).

REFERENCES AND NOTES

1. C. Y. Chung, H. Seo, K. C. Sonntag, A. Brooks, L. Lin, O. Isacson, Cell type-specific gene expression of midbrain dopaminergic neurons reveals molecules involved in their vulnerability and protection. *Hum. Mol. Genet.* **14**, 1709–1725 (2005).
2. J. N. Guzman, J. Sanchez-Padilla, D. Wokosin, J. Kondapalli, E. Ilijic, P. T. Schumacker, D. J. Surmeier, Oxidant stress evoked by pacemaking in dopaminergic neurons is attenuated by DJ-1. *Nature* **468**, 696–700 (2010).
3. T. G. Lesnick, S. Papapetropoulos, D. C. Mash, J. Ffrench-Mullen, L. Shehadeh, M. de Andrade, J. R. Henley, W. A. Rocca, J. E. Ahlskog, D. M. Maraganore, A genomic pathway approach to a complex disease: Axon guidance and Parkinson disease. *PLoS Genet.* **3**, e98 (2007).
4. J. W. Langston, P. Ballard, J. W. Tetrud, I. Irwin, Chronic parkinsonism in humans due to a product of meperidine-analog synthesis. *Science* **219**, 979–980 (1983).
5. J. M. Gorell, C. C. Johnson, B. A. Rybicki, E. L. Peterson, R. J. Richardson, The risk of Parkinson's disease with exposure to pesticides, farming, well water, and rural living. *Neurology* **50**, 1346–1350 (1998).
6. J. Simón-Sánchez, C. Schulte, J. M. Bras, M. Sharma, J. R. Gibbs, D. Berg, C. Paisan-Ruiz, P. Lichtner, S. W. Scholz, D. G. Hernandez, R. Krüger, M. Federoff, C. Klein, A. Goate, J. Perlmutter, M. Bonin, M. A. Nalls, T. Illig, C. Gieger, H. Houlden, M. Steffens, M. S. Okun, B. A. Racette, M. R. Cookson, K. D. Foote, H. H. Fernandez, B. J. Traynor, S. Schreiber, S. Arepalli, R. Zonozi, K. Gwinn, M. van der Brug, G. Lopez, S. J. Chanock, A. Schatzkin, Y. Park, A. Hollenbeck, J. Gao, X. Huang, N. W. Wood, D. Lorenz, G. Deuschl, H. Chen, O. Riess, J. A. Hardy, A. B. Singleton, T. Gasser, Genome-wide association study reveals genetic risk underlying Parkinson's disease. *Nat. Genet.* **41**, 1308–1312 (2009).
7. M. R. Cookson, O. Bandmann, Parkinson's disease: Insights from pathways. *Hum. Mol. Genet.* **19**, R21–R27 (2010).
8. J. Hardy, Genetic analysis of pathways to Parkinson disease. *Neuron* **68**, 201–206 (2010).
9. A. Zimprich, S. Biskup, P. Leitner, P. Lichtner, M. Farrer, S. Lincoln, J. Kachergus, M. Hulihan, R. J. Uitti, D. B. Calne, A. J. Stoessl, R. F. Pfeiffer, N. Patenge, I. C. Carbajal, P. Vieregge, F. Asmus, B. Müller-Myhsok, D. W. Dickson, T. Meitinger, T. M. Strom, Z. K. Wszolek, T. Gasser, Mutations in *LRRK2* cause autosomal-dominant parkinsonism with pleomorphic pathology. *Neuron* **44**, 601–607 (2004).
10. C. Paisán-Ruíz, S. Jain, E. W. Evans, W. P. Gilks, J. Simón, M. van der Brug, A. López de Munain, S. Aparicio, A. M. Gil, N. Khan, J. Johnson, J. R. Martinez, D. Nicholl, I. M. Carrera, A. S. Pena, R. de Silva, A. Lees, J. F. Martí-Massó, J. Pérez-Tur, N. W. Wood, A. B. Singleton, Cloning of the gene containing mutations that cause *PARK8*-linked Parkinson's disease. *Neuron* **44**, 595–600 (2004).
11. J. O. Aasly, M. Toft, I. Fernandez-Mata, J. Kachergus, M. Hulihan, L. R. White, M. Farrer, Clinical features of *LRRK2*-associated Parkinson's disease in central Norway. *Ann. Neurol.* **57**, 762–765 (2005).
12. D. G. Healy, M. Falchi, S. S. O'Sullivan, V. Bonifati, A. Durr, S. Bressman, A. Brice, J. Aasly, C. P. Zabetian, S. Goldwurm, J. J. Ferreira, E. Tolosa, D. M. Kay, C. Klein, D. R. Williams, C. Marras, A. E. Lang, Z. K. Wszolek, J. Berciano, A. H. Schapira, T. Lynch, K. P. Bhatia, T. Gasser, A. J. Lees, N. W. Wood; International LRRK2 Consortium, Phenotype, genotype, and worldwide genetic penetrance of *LRRK2*-associated Parkinson's disease: A case-control study. *Lancet Neurol.* **7**, 583–590 (2008).
13. A. S. Chen-Plotkin, W. Yuan, C. Anderson, E. McCarty Wood, H. I. Hurtig, C. M. Clark, B. L. Miller, V. M. Lee, J. Q. Trojanowski, M. Grossman, V. M. Van Deerlin, Corticobasal syndrome and

primary progressive aphasia as manifestations of *LRRK2* gene mutations. *Neurology* **70**, 521–527 (2008).
14. B. I. Giasson, J. P. Covy, N. M. Bonini, H. I. Hurtig, M. J. Farrer, J. Q. Trojanowski, V. M. Van Deerlin, Biochemical and pathological characterization of Lrrk2. *Ann. Neurol.* **59**, 315–322 (2006).
15. B. D. Lee, J. H. Shin, J. VanKampen, L. Petrucelli, A. B. West, H. S. Ko, Y. I. Lee, K. A. Maguire-Zeiss, W. J. Bowers, H. J. Federoff, V. L. Dawson, T. M. Dawson, Inhibitors of leucine-rich repeat kinase-2 protect against models of Parkinson's disease. *Nat. Med.* **16**, 998–1000 (2010).
16. M. R. Cookson, The role of leucine-rich repeat kinase 2 (*LRRK2*) in Parkinson's disease. *Nat. Rev. Neurosci.* **11**, 791–797 (2010).
17. E. M. Valente, P. M. Abou-Sleiman, V. Caputo, M. M. Muqit, K. Harvey, S. Gispert, Z. Ali, D. Del Turco, A. R. Bentivoglio, D. G. Healy, A. Albanese, R. Nussbaum, R. González-Maldonado, T. Deller, S. Salvi, P. Cortelli, W. P. Gilks, D. S. Latchman, R. J. Harvey, B. Dallapiccola, G. Auburger, N. W. Wood, Hereditary early-onset Parkinson's disease caused by mutations in *PINK1*. *Science* **304**, 1158–1160 (2004).
18. E. M. Valente, A. R. Bentivoglio, P. H. Dixon, A. Ferraris, T. Ialongo, M. Frontali, A. Albanese, N. W. Wood, Localization of a novel locus for autosomal recessive early-onset parkinsonism, *PARK6*, on human chromosome 1p35-p36. *Am. J. Hum. Genet.* **68**, 895–900 (2001).
19. Y. Hatano, K. Sato, B. Elibol, H. Yoshino, Y. Yamamura, V. Bonifati, H. Shinotoh, M. Asahina, S. Kobayashi, A. R. Ng, R. L. Rosales, S. Hassin-Baer, Y. Shinar, C. S. Lu, H. C. Chang, Y. H. Wu-Chou, F. B. Ataç, T. Kobayashi, T. Toda, Y. Mizuno, N. Hattori, PARK6-linked autosomal recessive early-onset parkinsonism in Asian populations. *Neurology* **63**, 1482–1485 (2004).
20. Y. Hatano, Y. Li, K. Sato, S. Asakawa, Y. Yamamura, H. Tomiyama, H. Yoshino, M. Asahina, S. Kobayashi, S. Hassin-Baer, C. S. Lu, A. R. Ng, R. L. Rosales, N. Shimizu, T. Toda, Y. Mizuno, N. Hattori, Novel *PINK1* mutations in early-onset parkinsonism. *Ann. Neurol.* **56**, 424–427 (2004).
21. K. Hedrich, J. Hagenah, A. Djarmati, A. Hiller, T. Lohnau, K. Lasek, A. Grünewald, R. Hilker, S. Steinlechner, H. Boston, N. Kock, C. Schneider-Gold, W. Kress, H. Siebner, F. Binkofski, R. Lencer, A. Münchau, C. Klein, Clinical spectrum of homozygous and heterozygous *PINK1* mutations in a large German family with Parkinson disease: Role of a single hit? *Arch. Neurol.* **63**, 833–838 (2006).
22. M. Kasten, C. Weichert, K. Lohmann, C. Klein, Clinical and demographic characteristics of *PINK1* mutation carriers—A meta-analysis. *Mov. Disord.* **25**, 952–954 (2010).
23. W. Satake, Y. Nakabayashi, I. Mizuta, Y. Hirota, C. Ito, M. Kubo, T. Kawaguchi, T. Tsunoda, M. Watanabe, A. Takeda, H. Tomiyama, K. Nakashima, K. Hasegawa, F. Obata, T. Yoshikawa, H. Kawakami, S. Sakoda, M. Yamamoto, N. Hattori, M. Murata, Y. Nakamura, T. Toda, Genome-wide association study identifies common variants at four loci as genetic risk factors for Parkinson's disease. *Nat. Genet.* **41**, 1303–1307 (2009).
24. Y. J. Edwards, G. W. Beecham, W. K. Scott, S. Khuri, G. Bademci, D. Tekin, E. R. Martin, Z. Jiang, D. C. Mash, J. ffrench-Mullen, M. A. Pericak-Vance, N. Tsinoremas, J. M. Vance, Identifying consensus disease pathways in Parkinson's disease using an integrative systems biology approach. *PLoS One* **6**, e16917 (2011).
25. C. Klein, R. Chuang, C. Marras, A. E. Lang, The curious case of phenocopies in families with genetic Parkinson's disease. *Mov. Disord.* **26**, 1793–1802 (2011).
26. M. A. Israel, S. H. Yuan, C. Bardy, S. M. Reyna, Y. Mu, C. Herrera, M. P. Hefferan, S. Van Gorp, K. L. Nazor, F. S. Boscolo, C. T. Carson, L. C. Laurent, M. Marsala, F. H. Gage, A. M. Remes, E. H. Koo, L. S. Goldstein, Probing sporadic and familial Alzheimer's disease using induced pluripotent stem cells. *Nature* **482**, 216–220 (2012).
27. P. Seibler, J. Graziotto, H. Jeong, F. Simunovic, C. Klein, D. Krainc, Mitochondrial Parkin recruitment is impaired in neurons derived from mutant PINK1 induced pluripotent stem cells. *J. Neurosci.* **31**, 5970–5976 (2011).
28. C. Vives-Bauza, C. Zhou, Y. Huang, M. Cui, R. L. de Vries, J. Kim, J. May, M. A. Tocilescu, W. Liu, H. S. Ko, J. Magrané, D. J. Moore, V. L. Dawson, R. Grailhe, T. M. Dawson, C. Li, K. Tieu, S. Przedborski, PINK1-dependent recruitment of Parkin to mitochondria in mitophagy. *Proc. Natl. Acad. Sci. U.S.A.* **107**, 378–383 (2010).
29. V. S. Van Laar, B. Arnold, S. J. Cassady, C. T. Chu, E. A. Burton, S. B. Berman, Bioenergetics of neurons inhibit the translocation response of Parkin following rapid mitochondrial depolarization. *Hum. Mol. Genet.* **20**, 927–940 (2011).
30. T. Brustovetsky, V. Li, N. Brustovetsky, Stimulation of glutamate receptors in cultured hippocampal neurons causes Ca^{2+}-dependent mitochondrial contraction. *Cell Calcium* **46**, 18–29 (2009).
31. T. Nishi, M. Forgac, The vacuolar (H^+)-ATPases—Nature's most versatile proton pumps. *Nat. Rev. Mol. Cell Biol.* **3**, 94–103 (2002).
32. S. Dröse, K. U. Bindseil, E. J. Bowman, A. Siebers, A. Zeeck, K. Altendorf, Inhibitory effect of modified bafilomycins and concanamycins on P- and V-type adenosinetriphosphatases. *Biochemistry* **32**, 3902–3906 (1993).
33. A. V. Zhdanov, R. I. Dmitriev, D. B. Papkovsky, Bafilomycin A1 activates respiration of neuronal cells via uncoupling associated with flickering depolarization of mitochondria. *Cell. Mol. Life Sci.* **68**, 903–917 (2011).
34. V. V. Teplova, A. A. Tonshin, P. A. Grigoriev, N. E. Saris, M. S. Salkinoja-Salonen, Bafilomycin A1 is a potassium ionophore that impairs mitochondrial functions. *J. Bioenerg. Biomembr.* **39**, 321–329 (2007).
35. A. Grünewald, G. J. Breedveld, K. Lohmann-Hedrich, C. F. Rohé, I. R. König, J. Hagenah, N. Vanacore, G. Meco, A. Antonini, S. Goldwurm, S. Lesage, A. Dürr, F. Binkofski, H. Siebner, A. Münchau, A. Brice, B. A. Oostra, C. Klein, V. Bonifati, Biological effects of the *PINK1* c.1366C>T mutation: Implications in Parkinson disease pathogenesis. *Neurogenetics* **8**, 103–109 (2007).
36. A. S. Divakaruni, M. D. Brand, The regulation and physiology of mitochondrial proton leak. *Physiology* **26**, 192–205 (2011).
37. A. B. West, D. J. Moore, S. Biskup, A. Bugayenko, W. W. Smith, C. A. Ross, V. L. Dawson, T. M. Dawson, Parkinson's disease-associated mutations in leucine-rich repeat kinase 2 augment kinase activity. *Proc. Natl. Acad. Sci. U.S.A.* **102**, 16842–16847 (2005).
38. G. Morfini, G. Pigino, K. Opalach, Y. Serulle, J. E. Moreira, M. Sugimori, R. R. Llinás, S. T. Brady, 1-Methyl-4-phenylpyridinium affects fast axonal transport by activation of caspase and protein kinase C. *Proc. Natl. Acad. Sci. U.S.A.* **104**, 2442–2447 (2007).
39. A. R. Saha, J. Hill, M. A. Utton, A. A. Asuni, S. Ackerley, A. J. Grierson, C. C. Miller, A. M. Davies, V. L. Buchman, B. H. Anderton, D. P. Hanger, Parkinson's disease α-synuclein mutations exhibit defective axonal transport in cultured neurons. *J. Cell Sci.* **117**, 1017–1024 (2004).
40. C. Y. Chung, J. B. Koprich, H. Siddiqi, O. Isacson, Dynamic changes in presynaptic and axonal transport proteins combined with striatal neuroinflammation precede dopaminergic neuronal loss in a rat model of AAV α-synucleinopathy. *J. Neurosci.* **29**, 3365–3373 (2009).
41. L. S. Goldstein, Z. Yang, Microtubule-based transport systems in neurons: The roles of kinesins and dyneins. *Annu. Rev. Neurosci.* **23**, 39–71 (2000).
42. F. Gillardon, Leucine-rich repeat kinase 2 phosphorylates brain tubulin-beta isoforms and modulates microtubule stability—A point of convergence in parkinsonian neurodegeneration? *J. Neurochem.* **110**, 1514–1522 (2009).
43. B. Frei, M. C. Kim, B. N. Ames, Ubiquinol-10 is an effective lipid-soluble antioxidant at physiological concentrations. *Proc. Natl. Acad. Sci. U.S.A.* **87**, 4879–4883 (1990).
44. P. C. Chin, L. Liu, B. E. Morrison, A. Siddiq, R. R. Ratan, T. Bottiglieri, S. R. D'Mello, The c-Raf inhibitor GW5074 provides neuroprotection in vitro and in an animal model of neurodegeneration through a MEK-ERK and Akt-independent mechanism. *J. Neurochem.* **90**, 595–608 (2004).
45. B. Dehay, J. Bové, N. Rodríguez-Muela, C. Perier, A. Recasens, P. Boya, M. Vila, Pathogenic lysosomal depletion in Parkinson's disease. *J. Neurosci.* **30**, 12535–12544 (2010).
46. C. Malagelada, Z. H. Jin, V. Jackson-Lewis, S. Przedborski, L. A. Greene, Rapamycin protects against neuron death in in vitro and in vivo models of Parkinson's disease. *J. Neurosci.* **30**, 1166–1175 (2010).
47. C. Malagelada, Z. H. Jin, L. A. Greene, RTP801 is induced in Parkinson's disease and mediates neuron death by inhibiting Akt phosphorylation/activation. *J. Neurosci.* **28**, 14363–14371 (2008).
48. L. S. Tain, H. Mortiboys, R. N. Tao, E. Ziviani, O. Bandmann, A. J. Whitworth, Rapamycin activation of 4E-BP prevents parkinsonian dopaminergic neuron loss. *Nat. Neurosci.* **12**, 1129–1135 (2009).
49. H. Mortiboys, K. K. Johansen, J. O. Aasly, O. Bandmann, Mitochondrial impairment in patients with Parkinson disease with the G2019S mutation in *LRRK2*. *Neurology* **75**, 2017–2020 (2010).
50. C. Piccoli, A. Sardanelli, R. Scrima, M. Ripoli, G. Quarato, A. D'Aprile, F. Bellomo, S. Scacco, G. De Michele, A. Filla, A. Iuso, D. Boffoli, N. Capitanio, S. Papa, Mitochondrial respiratory dysfunction in familiar parkinsonism associated with PINK1 mutation. *Neurochem. Res.* **33**, 2565–2574 (2008).
51. A. Rakovic, A. Grünewald, P. Seibler, A. Ramirez, N. Kock, S. Orolicki, K. Lohmann, C. Klein, Effect of endogenous mutant and wild-type PINK1 on Parkin in fibroblasts from Parkinson disease patients. *Hum. Mol. Genet.* **19**, 3124–3137 (2010).
52. A. Rakovic, A. Grünewald, J. Kottwitz, N. Brüggemann, P. P. Pramstaller, K. Lohmann, C. Klein, Mutations in PINK1 and Parkin impair ubiquitination of Mitofusins in human fibroblasts. *PLoS One* **6**, e16746 (2011).
53. P. Damier, E. C. Hirsch, Y. Agid, A. M. Graybiel, The substantia nigra of the human brain. II. Patterns of loss of dopamine-containing neurons in Parkinson's disease. *Brain* **122**, 1437–1448 (1999).
54. D. J. Brooks, Examining Braak's hypothesis by imaging Parkinson's disease. *Mov. Disord.* **25** (Suppl. 1), S83–S88 (2010).
55. A. Bender, K. J. Krishnan, C. M. Morris, G. A. Taylor, A. K. Reeve, R. H. Perry, E. Jaros, J. S. Hersheson, J. Betts, T. Klopstock, R. W. Taylor, D. M. Turnbull, High levels of mitochondrial DNA deletions in substantia nigra neurons in aging and Parkinson disease. *Nat. Genet.* **38**, 515–517 (2006).
56. Y. Kraytsberg, E. Kudryavtseva, A. C. McKee, C. Geula, N. W. Kowall, K. Khrapko, Mitochondrial DNA deletions are abundant and cause functional impairment in aged human substantia nigra neurons. *Nat. Genet.* **38**, 518–520 (2006).
57. A. Colman, O. Dreesen, Pluripotent stem cells and disease modeling. *Cell Stem Cell* **5**, 244–247 (2009).
58. K. Saha, R. Jaenisch, Technical challenges in using human induced pluripotent stem cells to model disease. *Cell Stem Cell* **5**, 584–595 (2009).
59. L. L. Rubin, Stem cells and drug discovery: The beginning of a new era? *Cell* **132**, 549–552 (2008).
60. Z. K. Wszolek, R. F. Pfeiffer, Y. Tsuboi, R. J. Uitti, R. D. McComb, A. J. Stoessl, A. J. Strongosky, A. Zimprich, B. Müller-Myhsok, M. J. Farrer, T. Gasser, D. B. Calne, D. W. Dickson, Autosomal

dominant parkinsonism associated with variable synuclein and tau pathology. *Neurology* **62**, 1619–1622 (2004).
61. L. Ishihara, L. Warren, R. Gibson, R. Amouri, S. Lesage, A. Dürr, M. Tazir, Z. K. Wszolek, R. J. Uitti, W. C. Nichols, A. Griffith, N. Hattori, D. Leppert, R. Watts, C. P. Zabetian, T. M. Foroud, M. J. Farrer, A. Brice, L. Middleton, F. Hentati, Clinical features of Parkinson disease patients with homozygous leucine-rich repeat kinase 2 G2019S mutations. *Arch. Neurol.* **63**, 1250–1254 (2006).
62. E. M. Chan, S. Ratanasirintrawoot, I. H. Park, P. D. Manos, Y. H. Loh, H. Huo, J. D. Miller, O. Hartung, J. Rho, T. A. Ince, G. Q. Daley, T. M. Schlaeger, Live cell imaging distinguishes bona fide human iPS cells from partially reprogrammed cells. *Nat. Biotechnol.* **27**, 1033–1037 (2009).
63. G. L. Boulting, E. Kiskinis, G. F. Croft, M. W. Amoroso, D. H. Oakley, B. J. Wainger, D. J. Williams, D. J. Kahler, M. Yamaki, L. Davidow, C. T. Rodolfa, J. T. Dimos, S. Mikkilineni, A. B. Macdermott, C. J. Woolf, C. E. Henderson, H. Wichterle, K. Eggan, A functionally characterized test set of human induced pluripotent stem cells. *Nat. Biotechnol.* **29**, 279–286 (2011).
64. M. Deleidi, G. Hargus, P. Hallett, T. Osborn, O. Isacson, Development of histocompatible primate-induced pluripotent stem cells for neural transplantation. *Stem Cells* **29**, 1052–1063 (2011).
65. H. Deng, W. Le, Y. Guo, C. B. Hunter, W. Xie, M. Huang, J. Jankovic, Genetic analysis of *LRRK2* mutations in patients with Parkinson disease. *J. Neurol. Sci.* **251**, 102–106 (2006).
66. O. Cooper, G. Hargus, M. Deleidi, A. Blak, T. Osborn, E. Marlow, K. Lee, A. Levy, E. Perez-Torres, A. Yow, O. Isacson, Differentiation of human ES and Parkinson's disease iPS cells into ventral midbrain dopaminergic neurons requires a high activity form of SHH, FGF8a and specific regionalization by retinoic acid. *Mol. Cell. Neurosci.* **45**, 258–266 (2010).
67. M. Frank-Kamenetsky, X. M. Zhang, S. Bottega, O. Guicherit, H. Wichterle, H. Dudek, D. Bumcrot, F. Y. Wang, S. Jones, J. Shulok, L. L. Rubin, J. A. Porter, Small-molecule modulators of Hedgehog signaling: Identification and characterization of Smoothened agonists and antagonists. *J. Biol.* **1**, 10 (2002).
68. J. K. Chen, J. Taipale, K. E. Young, T. Maiti, P. A. Beachy, Small molecule modulation of Smoothened activity. *Proc. Natl. Acad. Sci. U.S.A.* **99**, 14071–14076 (2002).
69. C. Y. Chung, H. Seo, K. C. Sonntag, A. Brooks, L. Lin, O. Isacson, Cell type-specific gene expression of midbrain dopaminergic neurons reveals molecules involved in their vulnerability and protection. *Hum. Mol. Genet.* **14**, 1709–1725 (2005).
70. J. Pruszak, W. Ludwig, A. Blak, K. Alavian, O. Isacson, CD15, CD24, and CD29 define a surface biomarker code for neural lineage differentiation of stem cells. *Stem Cells* **27**, 2928–2940 (2009).
71. J. Magrané, I. Hervias, M. S. Henning, M. Damiano, H. Kawamata, G. Manfredi, Mutant SOD1 in neuronal mitochondria causes toxicity and mitochondrial dynamics abnormalities. *Hum. Mol. Genet.* **18**, 4552–4564 (2009).

Acknowledgments: We thank J. Lash, a study coordinator from the Mayo Clinic Florida who was instrumental in assisting in recruitment of patients for this study and making the travel arrangements for them. **Funding:** This work was supported by a grant from the American Recovery and Reinvestment Act–NIH/National Institute of Neurological Disorders and Stroke (NINDS) (1RC2NS070276) and the NIH U24 grant (1U24NS078338-01) awarded to the PDiPS Cell Research Consortium. O.I., O.C., H.S., M.S., J.M., T.O., G.H., M.D., T.L., H.B. and E.P.-T. were supported by the Michael J. Fox Foundation, the Harvard Stem Cell Institute and the Miller Consortium for the Development of Nervous System Therapies, the Orchard Foundation, the Harold and Ronna Cooper family, the Consolidated Anti-Aging Foundation, and the Poul Hansen family. Z.K.W. was partially supported by the NIH/NINDS NS057567, P50NS072187, Mayo Clinic Florida (MCF) Research Committee CR program (MCF #90052030), Dystonia Medical Research Foundation, and a gift from Carl Edward Bolch Jr. and Susan Bass Bolch (MCF 90052031/PAU 90052). S.A., L. Chen, L.A.S., V.L.D., and T.M.D. were supported by NIH/NINDS NS38377 and the Maryland Stem Cell Research Foundation 2007-MSCRFI-0420-00 and acknowledge the joint participation by the Adrienne Helis Malvin Medical Research Foundation through its direct engagement in the continuous active conduct of medical research in conjunction with The Johns Hopkins Hospital and the Johns Hopkins University School of Medicine and the Foundation's Parkinson's Disease Program No. M-1. C.K. was supported by a career development award from the Hermann and Lilly Schilling Foundation. **Author contributions:** O.C., H.S., S.A., C.G.-L., J.G., M.S., J.R.M., L.C.-R., Z.X., T.O., G.H., M.D., T.L., H.B., E.P.-T., L. Clark, C.M., J.M., L. Chen, L.V.-D., N.R., H.J., R.J.U., Z.H., G.O., L.A.S., V.L.D., C.K., J.F., O.A.R., J.Q.T., V.M.-Y.L., K.M., D.J.S., Z.K.W., S.P., D.K., T.M.D., and O.I. contributed to the ideas and designs of the experiments. O.C., H.S., and O.I. designed the experiments and wrote the manuscript. O.C., H.S., M.S., T.O., G.H., and M.D. performed cytotoxicity assays. S.A., L.A.S., V.L.D., T.M.D., J.G., J.M., and D.K. designed, performed, and analyzed the OCRs of neural cells. O.C., H.S., M.S., M.D., T.L., and E.P.-T. performed the experiments using flow cytometry. C.G.-L., N.R., and S.P. designed, performed, and analyzed the mitochondrial dynamics in neurons. O.C., J.M., and O.I. performed and analyzed the genotyping and transgene silencing of the iPSC lines. L.C.-R., Z.X., and D.J.S. designed, performed, and analyzed the electrophysiological experiments for PD iPSC-derived neurons. O.C., M.S., T.O., G.H., M.D., T.L., H.B., and O.I. performed and analyzed differentiation experiments. L.C., C.M., R.J.U., Z.H., G.O., K.M., T.M.D., and Z.K.W. recruited and genotyped patients and created fibroblast samples. D.K. and C.K. provided the PINK1 PD patient and healthy subject iPSC lines. **Competing interests:** T.M.D. is a paid consultant to Merck KGAA, TEVA Pharmaceuticals, UptoDate Inc., Boehringer Ingelheim, Glaxo Research and Development LTD, Pfizer Inc., QRx Pharma, and Schering-Plough Research Institute. The terms of these arrangements are being managed by the Johns Hopkins University in accordance with its conflict of interest policies. Z.K.W. has a financial interest in a technology (LRRK2 gene test), which has been licensed to a commercial entity. Mayo Clinic and Z.K.W. receive royalties from that license. The other authors declare that they have no competing interests. **Data and materials availability:** The biological samples, fibroblasts, and iPSCs used are stored at the participating institutions and will also be stored at the NINDS Human Genetics DNA and Cell Line Repository at Coriell Institute for Medical Research.

Submitted 7 March 2012
Accepted 1 June 2012
Published 4 July 2012
10.1126/scitranslmed.3003985

Citation: O. Cooper, H. Seo, S. Andrabi, C. Guardia-Laguarta, J. Graziotto, M. Sundberg, J. R. McLean, L. Carrillo-Reid, Z. Xie, T. Osborn, G. Hargus, M. Deleidi, T. Lawson, H. Bogetofte, E. Perez-Torres, L. Clark, C. Moskowitz, J. Mazzulli, L. Chen, L. Volpicelli-Daley, N. Romero, H. Jiang, R. J. Uitti, Z. Huang, G. Opala, L. A. Scarffe, V. L. Dawson, C. Klein, J. Feng, O. A. Ross, J. Q. Trojanowski, V. M.-Y. Lee, K. Marder, D. J. Surmeier, Z. K. Wszolek, S. Przedborski, D. Krainc, T. M. Dawson, O. Isacson, Pharmacological rescue of mitochondrial deficits in iPSC-derived neural cells from patients with familial Parkinson's disease. *Sci. Transl. Med.* **4**, 141ra90 (2012).